Supporting Information

Yuan et al. 10.1073/pnas.1424962112

The Velocity Profile of the External Flow

The axial velocity profile (u) of a fully developed, laminar flow in a conduit with a rectangular cross-section is (1)

$$u(y,z)=\frac{4\mathrm{W}^2}{\mu\pi^3}\left(-\frac{dp}{dx}\right)\sum_{i=1,3,5,\ldots}^{\infty}(-1)^{\frac{(i-1)}{2}}\left[1-\frac{\cosh(i\pi z/\mathrm{W})}{\cosh(i\pi b/\mathrm{W})}\right]\frac{\cos(i\pi y/\mathrm{W})}{i^3}, \quad \textbf{[S1]}$$

where W, $2b$, and μ are, respectively, the conduit's width, the conduit's depth, and the liquid's dynamic viscosity. $-\mathrm{W}/2 < y < \mathrm{W}/2$. $-b < z < b$. The pressure gradient

$$-\frac{dp}{dx}=\frac{6\mu Q}{b\mathrm{W}^3}\frac{1}{1-\frac{96\mathrm{W}}{\pi^5 b}\sum_{i=1,3,5,\ldots}^{\infty}\frac{\tanh(i\pi b/\mathrm{W})}{i^5}}, \quad \textbf{[S2]}$$

where Q is the volumetric flow rate. The velocity averaged over the conduit's depth

$$\overline{u}(\mathrm{y})=\frac{\int_{-b}^{b}u(\mathrm{y},\mathrm{z})dz}{2b}. \quad \textbf{[S3]}$$

The infinite series in Eq. **S2** converges rapidly. In our calculations, we truncated the series after 100 terms. Fig. S1 depicts (*A*) contours of axial velocity and (*B*) the depth-averaged velocity as a function of distance from the side wall. The conduit's dimensions are the same as in our experiment (100 μm deep × 2.6 mm wide). The flow rate Q = 3,000 μL/h.

Numerical Simulations

Because 3D simulations are time-consuming and the essence of the rheotaxis phenomenon can be captured with a 2D model, we carried out direct, 2D numerical simulations with the finite element program COMSOL to examine whether we can replicate the phenomena that we observed in the experiments.

Because the Reynolds number associated with the swimming *Caenorhabditis elegans* is small, we solve the Stokes equation

$$-\nabla p+\mu\nabla^2\mathbf{u}=0. \quad \textbf{[S4]}$$

The liquid is incompressible and the velocity field satisfies the continuity equation

$$\nabla\cdot\mathbf{u}=0. \quad \textbf{[S5]}$$

In the above, $\mathbf{u}$ is the velocity vector and p is the pressure.

We define the local coordinates x_L and y_L with their origin at the center of mass of the swimmer. At any instant in time, the coordinate x_L is inclined with angle θ with respect to the conduit's axis. We approximate the *C. elegans* as a 2D, flexible, undulating sheet with a uniform cross-section. The position of the swimmer's skeleton

$$y_L=b\sin 2\pi\left(\frac{x_L}{\lambda}-ft\right) \quad \textbf{[S6]}$$

is a function of the axial position x_L. $0\le x_L\le\lambda$. In the above, λ is the wavelength of the undulating wave, b is the amplitude, and f is the frequency. The swimmer's thickness, wavelength, amplitude, and frequency were set, respectively, to 69 μm, 1,005 μm, 112.5 μm, and 1.7 Hz to match the corresponding characteristics of the actual swimmer. The swimmer is confined in a conduit $-W/2 < y < W/2$, where W = 2.6 mm is the conduit's width.

The swimmer translates with instantaneous horizontal (U) and vertical (V) velocities as well as rotates with angular velocity ω around its center of mass. All these velocities are not known a priori and must be obtained as part of the solution process. The boundary conditions consist of specified axial and vertical undulating wave velocities along the swimmer's body:

$$u_x=U-y\omega+2\pi fb\cos 2\pi\left(\frac{x}{\lambda}-ft\right)\sin\theta \quad \textbf{[S7]}$$

and

$$u_y=V-x\omega-2\pi fb\cos 2\pi\left(\frac{x}{\lambda}-ft\right)\cos\theta. \quad \textbf{[S8]}$$

Additionally, we specified a parabolic velocity profile with an average of 300 μm/s at the conduit's inlet, zero outlet viscous stress, and nonslip conditions at all solid surfaces. Both the conduit's inlet and outlet were located more than five wavelengths away from the swimmer's center of mass so that the locations of the inlet and outlet had negligible effect on the computational results.

The instantaneous hydrodynamic force and torque are, respectively,

$$\mathbf{F}=\oiint_s\left(-p\mathbf{I}+\mu\left(\nabla\mathbf{u}^T+\nabla\mathbf{u}\right)\right)\hat{\mathbf{n}}ds \quad \textbf{[S9]}$$

and

$$\boldsymbol{\tau}=\oiint_s\mathbf{r}\times\left(-p\mathbf{I}+\mu\left(\nabla\mathbf{u}^T+\nabla\mathbf{u}\right)\right)\hat{\mathbf{n}}ds. \quad \textbf{[S10]}$$

In the above, $\mathbf{r}$ is the radius vector from the swimmer's center of mass to a point on the animal's surface and $\hat{\mathbf{n}}$ is an outward unit vector on the swimmer's surface. The integration is carried out along the swimmer's surface. $\mathbf{I}$ is the unit tensor.

To prevent the swimmer from penetrating the side walls, we included a short-range repulsive (steric) force between the swimmer and the solid boundaries. To this end, discs (n = 21) were distributed along the swimmer's skeleton and a fast-decaying force was defined between each disk and the solid boundaries:

$$F_{LJ,i}(y_{sp,i})=\begin{cases}\varepsilon\left[2\left(\frac{\sigma}{\sigma_{tW}}\right)^{13}-\left(\frac{\sigma}{\sigma_{tW}}\right)^{7}\right], & \left(y_{tW}-rhsp-rsp<y_{sp,i}<y_{tW}-rhsp-2^{1/6}\sigma\right)\\ 0, & \left(y_{bW}+rhsp+rsp\le y_{sp,i}\le y_{tW}-rhsp-rsp\right)\\ -\varepsilon\left[2\left(\frac{\sigma}{\sigma_{bW}}\right)^{13}-\left(\frac{\sigma}{\sigma_{bW}}\right)^{7}\right], & \left(y_{bW}+rhsp+2^{1/6}\sigma<y_{sp,i}<y_{bW}+rhsp+rsp\right)\end{cases}. \quad \textbf{[S11]}$$

In the above, $F_{LJ,i}$ is the repulsive force experienced by the i^{th} disk and y_{sp}, y_{tw}, and y_{bw} are, respectively, the vertical coordinates of the discs, the top boundary, and the bottom boundary. $\sigma_{tw} = y_{tW} - y_{sp,i} - rhsp$. $\sigma_{bW} = y_{sp,i} - y_{bW} - rhsp$. In the simulations, we set $\varepsilon = 3.75 \times 10^8$ N/m, $\sigma = 1$ µm, $rsp = 138$ µm, and $rhsp = 39.5$ µm.

The total force and torque acting on the swimmer due to the above repulsive force are, respectively,

$$F_{LJ}(t) = \sum_{i=1}^{n} F_{LJ,i}(t) \quad \textbf{[S12]}$$

and

$$\tau_{LJ}(t) = \sum_{i=1}^{n} \mathbf{r}_i \times \mathbf{F}_{LJ,i}, \quad \textbf{[S13]}$$

where $\mathbf{r}_i$ is the distance vector from the swimmer's center of mass to the i^{th} disk's center.

The unknown instantaneous translational velocities U and V and the angular velocity ω are determined by requiring that no net force and no net torque act on the swimmer. Because the problem is linear, we use superposition. We construct four auxiliary problems such that the sum of the solutions of these problems is equivalent to the solution of the original problem. The velocity fields associated with the auxiliary problems I, II, III, and IV are denoted, respectively, as $\mathbf{u}_{\mathrm{I}}$, $\mathbf{u}_{\mathrm{II}}$, $\mathbf{u}_{\mathrm{III}}$, and $\mathbf{u}_{\mathrm{IV}}$. Each of the above velocity fields satisfies Eqs. **S4** and **S5**. The four auxiliary problems differ in the velocity conditions specified along the swimmer's surface and the conduit's inlet.

Problem I:

$$u_{I,x} = 1, \text{ and } u_{I,y} = 0. \quad \textbf{[S14]}$$

Problem II:

$$u_{II,x} = 0, \text{ and } u_{II,y} = 1. \quad \textbf{[S15]}$$

Problem III:

$$u_{III,x} = -y, \text{ and } u_{III,y} = -x. \quad \textbf{[S16]}$$

Problem IV:

$$\begin{aligned} u_{IV,x} &= 2\pi f b \cos 2\pi\left(\frac{x}{\lambda} - ft\right)\sin\theta \text{ and} \\ u_{IV,y} &= -2\pi f b \cos 2\pi\left(\frac{x}{\lambda} - ft\right)\cos\theta. \end{aligned} \quad \textbf{[S17]}$$

In the first three auxiliary problems, we specified zero velocity at the conduit's inlet and zero viscous stress at the conduit's outlet. In the last auxiliary problem, we specified a parabolic velocity profile with an average of 300 µm/s at the conduit's inlet and zero viscous stress at the conduit's outlet. Each of the four auxiliary problems has well-defined boundary conditions and can be solved independently. Once the auxiliary problems have been solved, we calculate the corresponding instantaneous hydrodynamic forces and torques acting on the swimmer. The instantaneous steric forces and torques are calculated using Eqs. **S11** and **S12**. We denote the various forces and torques associated with problems I, II, III, and IV as $F_{I,x}$,$F_{I,y}$,τ_I; $F_{II,x}$,$F_{II,y}$,τ_{II}; $F_{III,x}$, $F_{III,y}$,τ_{III}; and $F_{IV,x}$,$F_{IV,y}$, and τ_{IV}. We denote the steric force and torque as F_{LJ} and τ_{LJ}.

The complete solution of the original problem is given by the weighted sum of the solutions of the auxiliary problems:

$$\mathbf{u} = U\mathbf{u}_I + V\mathbf{u}_{II} + \Omega\mathbf{u}_{III} + \mathbf{u}_{IV}. \quad \textbf{[S18]}$$

The forces and torques acting on the swimmer are

$$F_x = UF_{I,x} + VF_{II,x} + \omega F_{III,x} + F_{IV,x}, \quad \textbf{[S19]}$$

$$F_y = UF_{I,y} + VF_{II,y} + \omega F_{III,y} + F_{IV,y} + F_{LJ}, \quad \textbf{[S20]}$$

and

$$\tau = U\tau_I + V\tau_{II} + \omega\tau_{III} + \tau_{IV} + \tau_{LJ}. \quad \textbf{[S21]}$$

The unknown instantaneous velocities (U, V) and angular velocity (ω) are determined by setting the net forces and torques to zero:

$$F_x = F_y = \tau = 0. \quad \textbf{[S22]}$$

To obtain the swimmer's trajectory and orientation, we solve the kinematic equations

$$\begin{pmatrix} \dot{X}(t) \\ \dot{Y}(t) \\ \dot{\theta}(t) \end{pmatrix} = \begin{pmatrix} U(t) \\ V(t) \\ \omega(t) \end{pmatrix}. \quad \textbf{[S23]}$$

The time step used in the numerical calculations was always smaller than 0.01 s (1.7% of the swimming period).

To verify the numerical code, we calculated the swimming speed of an infinitely long waving sheet and compared the numerical solution with Taylor's analysis (2). In our computer model we used periodic boundary conditions at the two ends of the swimmer, effectively rendering the swimmer infinite in length. The other boundaries of the computational domain were set far enough from the swimmer to render variations in the locations of the boundaries insignificant. Because Taylor's solution is valid only when the ratio between the gait amplitude (b) and the wavelength (λ) is small, we expect a good agreement between our simulation results and Taylor's solution only when $b/\lambda << 1$. Fig. S2 depicts the swimmer's velocity (U) normalized with the wave velocity (V_W) as a function of the dimensionless gait amplitude λ. Our predicted velocity (red circles) agrees well with Taylor's analytical solution (blue line) when $b/\lambda < 0.06$.

As another test, we considered a waving infinite sheet centered between two parallel, infinite plates. The analytical solution for this problem has been obtained by Katz (3), using lubrication approximation. Fig. S3 depicts the propulsive speed normalized with the wave speed as a function of W/(2b). $b/\lambda = 0.03$. The symbols and solid line correspond, respectively, to the finite element predictions and Katz's analytical solution. The two solutions are in good agreement.

1. White FM (1991) *Viscous Fluid Flow* (McGraw-Hill, New York), 2nd Ed, p 120.
2. Taylor GI (1951) Analysis of the swimming of microscopic organisms. *Proc R Soc Lond A Math Phys Sci* 209(1099):447–461.
3. Katz DF (1974) On the propulsion of micro-organisms near solid boundaries. *J Fluid Mech* 64(1):33–49.

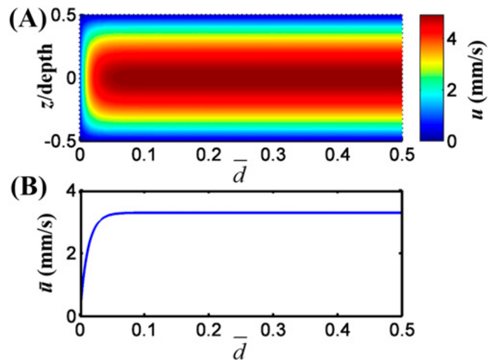

Fig. S1. The velocity contours (*A*) and the depth-averaged velocity as a function of normalized distance from the side surface (*B*) in a uniform rectangular conduit with the cross-sectional dimensions of our experimental apparatus.

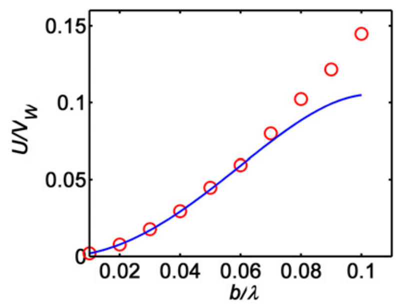

Fig. S2. The predicted swimming speed of an infinite length waving sheet in an infinite medium predicted by COMSOL (red circles) and Taylor's analytical solution (blue line) as a function of the gait's amplitude normalized with the wavelength.

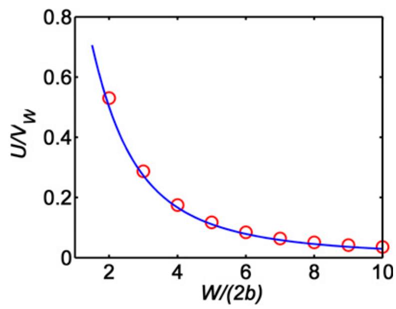

Fig. S3. The velocity of a waving, confined, infinite sheet normalized with the wave speed as a function of the conduit's half-width normalized with the wave amplitude. $b/\lambda = 0.03$. The hollow circles and the solid line correspond, respectively, to the finite element solution and Katz's analytical solution.

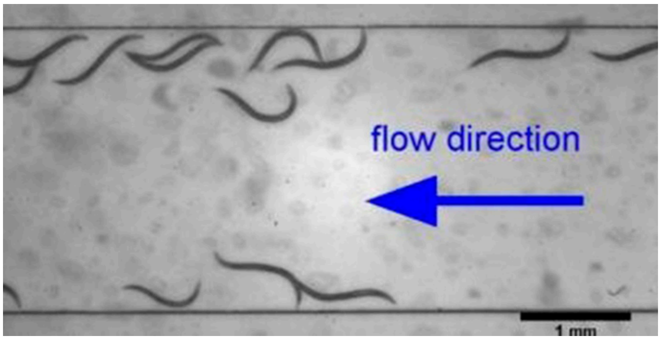

Movie S1. Young adults migrating upstream in the presence of mild external flow (300 μL/h, 321 μm/s) in a 2.6-mm-wide conduit. Animals swimming along the side surfaces occasionally exhibit synchronized motion. The flow is to the left. Play speed: 2× real time. There are more animals near the top of the channel than its bottom, probably owing to the conduit inlet's being closer to the channel's top than to its bottom. (Scale bar: 1 mm.)

Movie S1

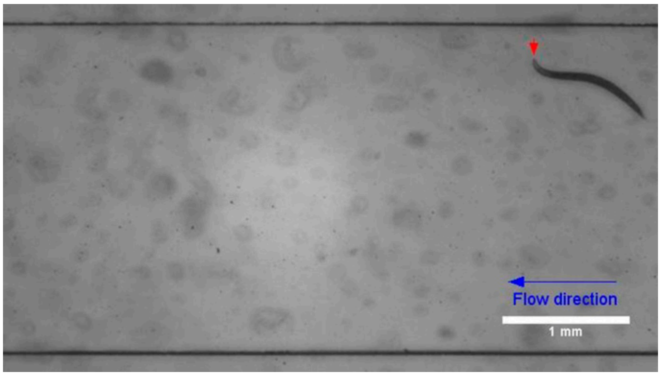

Movie S2. A young adult drifting in a high-velocity stream (3,000 μL/h, 3,210 μm/s) when near the conduit boundary. The conduit is 2.6 mm wide. Red arrows indicate the position of the animal's head. The flow is to the left. Play speed: real time. (Scale bar: 1 mm.)

Movie S2

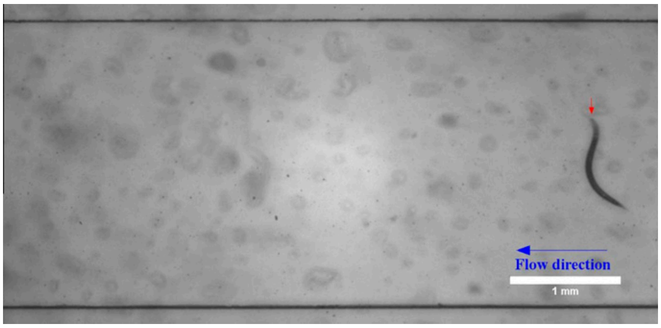

Movie S3. A young adult drifting in a high velocity stream (3,000 μL/h, 3,210 μm/s) when away from the conduit's boundary. The conduit is 2.6 mm wide. Red arrows indicate the position of the animal's head. The flow is to the left. Play speed: real time. (Scale bar: 1mm.)

Movie S3

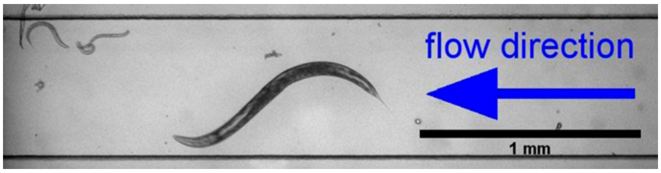

Movie S4. A young adult swimming in a fluid stream (460 μL/h, 2,130 μm/s) in a 0.6-mm-wide conduit. The conduit width is too small to accommodate hydrodynamically induced rotation but wide enough for the animals to make deliberate turns. The flow is to the left. Play speed: 0.5× real time. (Scale bar: 1mm.)

Movie S4

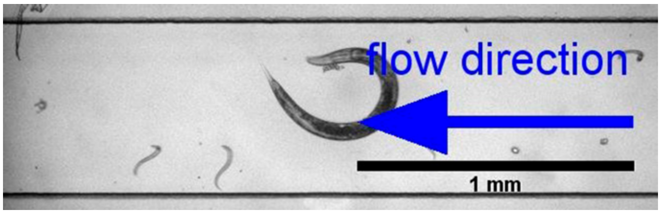

Movie S5. A young adult performing an omega turn in a fluid stream (460 μL/h, 2,130 μm/s) in a conduit whose width (0.6 mm) is smaller than the length of the animal (~1 mm). The flow is to the left. Play speed: 0.5× real time. (Scale bar: 1 mm.)

Movie S5

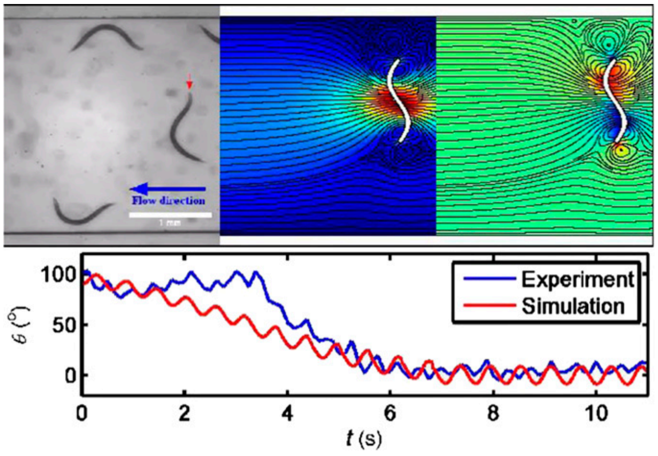

Movie S6. Comparison of computer simulations and experimental observations. Play speed: real time. (*Left*, experiment). Young adult *C. elegans* reorients to face against the flow in a mild fluid flow (300 μL/h, 321 μm/s). Red arrows denote the animal's head. The flow is directed to the left. (Scale bar: 1 mm.) (*Middle*) Numerical computations of a swimmer reorienting itself in the presence of external flow. The velocity magnitude is color-coded and the instantaneous streamlines are depicted as black lines. The flow is to the left. (*Right*) Numerical computations of a swimmer reorienting itself in the presence of external flow. The vorticity field is color-coded and the instantaneous streamlines are depicted as black lines. The flow is to the left. (*Bottom*) The swimmer's orientation (θ) as a function of time in the experiments (blue line) and the computer simulations (red line) are depicted as functions of time.

Movie S6